Nonradiative decay pathways of electronic states of group IV tetrafluoro and tetrachloro molecular ions studied with synchrotron radiation

Creasey, J. C.; Lambert, I. R.; Tuckett, R. P.; Codling, K.; Frasinski, L. J.; Hatherly, P. A.; Stankiewicz, M.; Holland, D. M. P.

DOI:
10.1063/1.458810

Nonradiative decay pathways of electronic states of group IV tetrafluoro and tetrachloro molecular ions studied with synchrotron radiation

J. C. Creasey, I. R. Lambert, and R. P. Tuckett
School of Chemistry, University of Birmingham, Edgbaston, Birmingham BI5 2TT, United Kingdom

K. Codling, L. J. Frasinski, P. A. Hatherly, and M. Stankiewicz
J. J. Thomson Physical Laboratory, University of Reading, Whiteknights, Reading RG6 2AF, United Kingdom

D. M. P. Holland
Science and Engineering Research Council Daresbury Laboratory, Warrington, Cheshire WA4 4AD, United Kingdom

(Received 15 February 1990; accepted 16 May 1990)

The nonradiative decay channels of the valence electronic states of the gas-phase tetrahedral ions CF_4^+, SiF_4^+, CCl_4^+, $SiCl_4^+$, and $GeCl_4^+$ have been studied in the range 35–100 nm by a novel form of photoionization mass spectrometry. Tunable vacuum UV radiation from a synchrotron source ionizes the parent neutral molecule, and electrons and ions are detected by the photoelectron–photoion coincidence technique. The experiment is repeated continuously as a function of photon energy, and a three-dimensional histogram of photon energy versus ion time of flight versus coincidence count rate is produced. By taking cuts through this histogram, photoionization curves for the different fragment ions can be extracted. The appearance energies of the fragment ions (e.g., CF_2^+ from CF_4, CCl^+ from CCl_4) occur at the adiabatic ionization potential of an electronic state of the parent ion, and not at the thermodynamic appearance energy of that ion. Attempts to measure the kinetic-energy releases in the fragmentation pathways have only been partially successful. The results are complementary to those of recent experiments to probe the radiative decay of these electronic states of MX_4^+ [M = C, Si, Ge; X = F, Cl] [J. Chem. Phys. **89**, 2675 (1988); **89**, 2683 (1988)], where the $\tilde{C}\,^2T_2$ and $\tilde{D}\,^2A_1$ third and fourth excited electronic states can show radiative decay to a surprising degree. The decay dynamics of the $\tilde{C}$ and $\tilde{D}$ states of MX_4^+ are reviewed. In general, the fluorides show different behavior to the analogous chlorides, and the carbon species behaves differently to the corresponding silicon or germanium species.

I. INTRODUCTION

In a series of papers,[1–4] we have reported the observation of electronic emission spectra of several group IV tetrahalide molecular ions MX_4^+ (M = C, Si, Ge; X = F, Cl) in the gas phase. The spectra are observed at a low rotational temperature in a crossed molecular-beam electron-beam apparatus. For the three fluorides CF_4^+, SiF_4^+, and GeF_4^+, both continuous and discrete bands have been observed in the ultraviolet to visible region of the electromagnetic spectrum. It is believed that the ground and first two excited states of these ions dissociate directly to $MF_3^+ + F$ [this has been confirmed for CF_4^+ (Refs. 5 and 6)], and the continuous bands arise from transitions to these states.[7–9] The discrete band arises from a transition between the fourth and third excited electronic states $\tilde{D}\,^2A_1$–$\tilde{C}\,^2T_2$, both of which are bound.[1–3] Computer simulation of the rotational band contour has confirmed that the observed vibronic bands are indeed due to a $^2A_1$–$^2T_2$ transition of a tetrahedral molecule observed at a low rotational temperature.[10,11] The excited electronic states of the three chlorides CCl_4^+, $SiCl_4^+$, and $GeCl_4^+$ show different decay properties. The $\tilde{X}$, $\tilde{A}$, and $\tilde{B}$ states probably all dissociate to $MCl_3^+ + Cl$. The $\tilde{C}$ state of $SiCl_4^+$ and $GeCl_4^+$ decays radiatively, whereas CCl_4^+ $\tilde{C}$ decays nonradiatively. The $\tilde{D}$ state of these ions does not fluoresce to any measurable extent.[4] Thus radiative decay is only observed as continuous, bound–free transitions in $SiCl_4^+$ and $GeCl_4^+$. Discrete spectra arising from transitions between two bound states are not observed, and thus high-resolution spectroscopic parameters have not been obtained for the $\tilde{C}\,^2T_2$ or $\tilde{D}\,^2A_1$ states of MCl_4^+.

These spectra are unusual in that emission is observed from excited electronic states which lie up to several eV above many dissociation channels. For such sized five-atom polyatomics, nonradiative processes would be expected to dominate, thus the observation of radiative decay at all is surprising. Indeed some of the bands in CF_4^+ have been incorrectly assigned to emission from smaller fragments.[12,13] We believe that the dynamics of the decay pathways of these excited electronic states are related to their spectroscopic properties, thus a full study of the competing radiative and nonradiative processes is needed. Using vacuum UV radiation from a synchrotron as a tunable photoionization source, we recently described experiments to probe radiative decay from the $\tilde{C}$ and $\tilde{D}$ states of MX_4^+.[4,14] Such experiments give energy thresholds, estimates of the fluorescence quantum yield $\Phi_{h\nu}$, and the lifetimes τ of the fluorescing states. Since $\Phi_{h\nu} = k_{\rm rad}/(k_{\rm rad} + k_{\rm nonrad})$ and $\tau^{-1} = k_{\rm rad} + k_{\rm nonrad}$ (where k is a decay rate), changes in $\Phi_{h\nu}$ and τ with excitation energy are especially interesting, since they can be attributed to a change in $k_{\rm nonrad}$ to a fragmentation channel. However, these channels are not probed direct-

 0021-9606/90/173295-12$03.00

ly. In this paper we describe the complementary experiments to probe these nonradiative decay processes. A gas jet of MX_4 is photoionized with radiation from the synchrotron source at the center of a pair of identical time-of-flight (TOF) mass spectrometers. Electrons are counted in delayed coincidence with photoions by the photoelectron–photoion coincidence (PEPICO) technique,[15] and a TOF mass spectrum is obtained. This is repeated continuously as a function of photon energy, and the energies at which the different fragmentation channels turn on can be obtained. This technique has many similarities to photoionization mass spectrometry (PIMS),[16] but with two main advantages. First, the use of a synchrotron source means that in our experiment wavelengths down to 350 Å can be accessed, whereas most PIMS experiments use a helium continuum and vacuum UV monochromator as the photon source with wavelengths limited to $\sim\lambda > 600$ Å. Second, the use of TOF detection means that all the fragment ions are collected simultaneously, and quantitative comparisons can be made between different ions collected in a single experiment (see Sec. VI).

Section II describes the apparatus in detail. Section III gives a résumé of the molecular orbitals of MX_4, the nature of the five valence electronic states of MX_4^+, and the energetics of the dissociation channels; these data are given in more detail elsewhere.[4,14] Section IV shows results for the five molecular ions we have studied in detail by this technique (CF_4^+, SiF_4^+, CCl_4^+, $SiCl_4^+$, and $GeCl_4^+$). Section V describes attempts to determine the kinetic-energy release for the different fragmentation channels from the widths of the fragment ion peaks in the TOF spectra. Section VI discusses the results, and places them in the context of our previous studies of radiative decay in excited electronic states of MX_4^+.[4,14] Section VII makes some general concluding remarks.

II. EXPERIMENT

The experiments were performed at the Science and Engineering Research Council Daresbury Synchrotron Radiation Source, and the apparatus has been described briefly elsewhere.[17,18] This apparatus has been used to study photofragmentation of doubly charged molecular ions, but it has proved relatively easy to adapt it to study fragmentation of the singly charged MX_4^+ ions with a continuously tunable photon energy. In essence, it now comprises a pair of identical TOF mass spectrometers connected to a tunable photoionization source (Fig. 1). Gas is admitted through a long, thin (i.d. = 0.5 mm) polytetrafluoro ethylene (PTFE) tube to a stainless-steel chamber which is pumped by a 330 liters s^{-1} turbo molecular pump. The base pressure of the chamber is 5×10^{-7} Torr, and with gas flowing the bulk pressure is typically 2×10^{-5} Torr. The gas is crossed orthogonally by tunable synchrotron radiation dispersed from a 1 m vacuum UV Seya monochromator (pressure = 10^{-9} Torr) equipped with a 1200 lines mm^{-1} grating blazed at 60 nm. Since we use wavelengths well below the LiF cutoff (the range of the monochromator being 100–35 nm), the radiation is focused out of the exit slit of the Seya into a 2 mm i.d.,

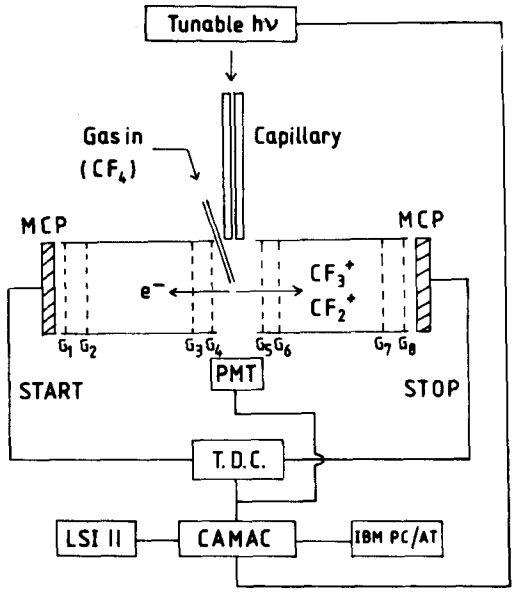

FIG. 1. Diagram of the apparatus G_1–G_8 are grids on the pair of identical TOF mass spectrometers. MCP = multichannel plates, PMT = photomultiplier tube, and TDC = time-to-digital converter.

100 mm long glass capillary which ends approximately 10 mm from the center of the TOF mass spectrometers. This capillary channels the radiation to the interaction region, ensures poor conductance between monochromator and experiment, and thus one stage of differential pumping (100 liters s^{-1} turbo) between the Seya and the chamber is sufficient to maintain the necessary, low pressure of the monochromator. The intensity of the radiation (bandwidth of 2 Å in all the experiments or 0.1 eV at 25 eV) is monitored by a window coated with sodium salicylate plus a photomultiplier tube (EMI 9789B) used in the photon counting mode. Photoionization products are detected by two pairs of 50 mm diam microchannel plates (Mullard G25-50) placed at the end of two identical drift tubes, each of length 70 mm. The grid configuration and potentials are arranged so that the ions are detected close to the spatial focusing condition.[19] The axes of the two drift tubes lie along the E vector of the almost 100% linearly polarized synchrotron radiation.

An electric field of 77 V cm^{-1} applied across the 2 cm interaction region accelerates photoelectrons to one pair of microchannel plates, photoions to the other. The electron and ion pulses are fed to a LeCroy 4208 time-to-digital converter (TDC) with a time resolution of 1 ns. The electrons provide the "start" pulse, ions the "stop" pulse, and the two are detected in delayed coincidence by the PEPICO technique.[15] The TOF data are processed using a bit-slice processor built by the Daresbury Laboratory and stored in a 64 kbyte memory module. The CAMAC crate is interfaced to two interacting computers, an IBM-PC/AT with EGA colour graphics and an LSI 11/23. The former sets the experimental parameters, displays the data in real time, and stores it on disk. Data accumulates as a three-dimensional histogram of photon energy versus ion TOF versus coincidence count rate,, with the last variable being represented by color.

The LSI 11 drives the Seya monochromator, stores the total electron count (amongst other auxiliary measurements), and accesses the main Daresbury CONVEX computer and the JANET inter-University network.

To display data from the IBM PC, cross-sectional cuts are taken through the three-dimensional histogram in one of two ways. Either, intensity versus TOF is displayed at a fixed photon energy, or the intensity of a particular fragment ion is shown as a function of photon energy. If the signal-to-noise ratio is high enough, the latter method is more revealing because it gives directly the energy at which the fragment ions turn on, and this can often be related to nonradiative decay of a particular electronic state of the parent ion MX_4^+. The former method is useful for seeing the turn-on of a weak fragmentation process (by comparing TOF spectra above and below a certain energy), but this energy is not uniquely defined. The original three-dimensional color spectra can be found elsewhere.[20]

The starting wavelength of the monochromator and the wavelength increment are two of the input parameters to the IBM PC at the start of an experiment. TOF spectra can be recorded at up to 128 values of the photoionization wavelength before the data has to be stored. Thus working at a resolution of 2 Å, a typical scan might be 500–564 Å (i.e. 24.8–22.0 eV) with the step size set to one-quarter (i.e., 0.5 Å *or* 0.02_2 eV) of the resolution. At each wavelength, a TOF spectrum accumulates until the number of counts from the photomultiplier tube behind the sodium salicylate coated window reaches a preset value. When this "flag" is reached, the LSI 11 steps on the Seya monochromator and the process is repeated. In this way we record TOF spectra which are normalized to the (changing) synchrotron flux. The initial total electron and ion count rates are set at 1000–2000 s^{-1}. For greater values, false coincidences degrade the signal-to-noise ratio; for smaller values, the signal-to-noise ratio can be poor unless the photomultiplier tube flag is set so high that accumulation times become unacceptably long.

Pure CF_4 and SiF_4 gas were supplied by the British Oxygen Company Ltd. and used without further purification. The three chlorides are all liquids at room temperature, and were supplied by Aldrich Chemical Co. After several freeze–pump–thaw cycles, their vapor pressure was admitted to the chamber from a glass container whose temperature was maintained at 293 K. Unfortunately, it was not possible to study GeF_4 in this apparatus for two reasons. First, our homemade sample (14% premixed in helium[3,14]) had a poisoning effect on the microchannel plates. Second, it was not possible to record a reliable TOF spectrum at any wavelength because the start and stop pulses were not correlated. Almost certainly this is due to collisions with helium "scrambling" the electron and ion time correlations.

We conclude this experimental section by commenting that the principle advantage of this apparatus over most TOF mass spectrometers is that it operates with a continuously tunable photoionization source. Thus the thresholds for production of the different fragment ions can be determined. Its principle limitation is that there is at present no energy analysis of the electrons (unlike more conventional PEPICO experiments using a fixed frequency source, e.g.,

TABLE I. Energetics of dissociation channels of CF_4^+, SiF_4^+, CCl_4^+, $SiCl_4^+$, and $GeCl_4^+$ in eV.

Neutral/parent ion	Dissociation channel	Energy (eV)[a]	Reference
CF_4^+ $\tilde{D}\,^2A_1$		25.1_2	21
	$CF_2 + F_2^+$	23.3	
	$CF_3 + F^+$	22.9	
	$CF^+ + F + F_2$	22.1	
$\tilde{C}\,^2T_2$		21.7_0	21
	$CF_2^+ + F + F$	20.8	
	$CF_2^+ + F_2$	19.2	
$\tilde{B}\,^2E$		18.3_0	21
$\tilde{A}\,^2T_2$		17.1_0	21
CF_4^+ $\tilde{X}\,^2T_1$		15.3_5	21
	$CF_3^+ + F$	14.7	
CF_4 $\tilde{X}\,^1A_1$		0	
	$SiF_2 + F_2^+$	26.3	
	$SiF^+ + F + F_2$	24.6	
	$SiF_3 + F^+$	24.3	
	$SiF_2^+ + F + F$	23.0	
SiF_4^+ $\tilde{D}\,^2A_1$		21.5_5	22
	$SiF_2^+ + F_2$	21.4	
$\tilde{C}\,^2T_2$		19.3_0	23
$\tilde{B}\,^2E$		18.0_0	23
$\tilde{A}\,^2T_2$		17.3_0	23
	$SiF_3^+ + F$	16.2	
SiF_4^+ $\tilde{X}\,^2T_1$		16.1_0	23
SiF_4 $\tilde{X}\,^1A_1$		0	
CCl_4^+ $\tilde{D}\,^2A_1$		19.9_0[b]	24
$\tilde{C}\,^2T_2$		16.3_4	25
	$CCl^+ + Cl + Cl_2$	16.3	
	$CCl_3 + Cl^+$	16.0	
	$CCl_2^+ + Cl + Cl$	15.8	
	$CCl_2 + Cl_2^+$	15.0	
	$CCl_2^+ + Cl_2$	13.3	
$\tilde{B}\,^2E$		13.3_7	25
$\tilde{A}\,^2T_2$		12.2_7	25
	$CCl_3^+ + Cl$	11.8	
CCl_4^+ $\tilde{X}\,^2T_1$		11.4_7	25
CCl_4 $\tilde{X}\,^1A_1$		0	
$SiCl_4^+$ $\tilde{D}\,^2A_1$		17.8_5	25
	$SiCl_3 + Cl^+$	17.8	
	$SiCl_2^+ + Cl + Cl$	17.7	
	$SiCl^+ + Cl + Cl_2$	16.8	
	$SiCl_2 + Cl_2^+$	16.6	
	$SiCl_2^+ + Cl_2$	15.2	
$\tilde{C}\,^2T_2$		15.0_9	25
$\tilde{B}\,^2E$		13.5_1	25
$\tilde{A}\,^2T_2$		12.7_5	25
	$SiCl_3^+ + Cl$	12.7	
$SiCl_4^+$ $\tilde{X}\,^2T_1$		11.7_9	25
$SiCl_4$ $\tilde{X}\,^1A_1$		0	
$GeCl_4^+$ $\tilde{D}\,^2A_1$		18.2_1	25
	$GeCl_2^+ + Cl + Cl$	16.0	
	$GeCl_3 + Cl^+$	15.8	
	$GeCl^+ + Cl + Cl_2$	15.1	
	$GeCl_2 + Cl_2^+$	14.8	
$\tilde{C}\,^2T_2$		14.5_6	25
	$GeCl_2^+ + Cl_2$	13.5	
$\tilde{B}\,^2E$		13.0_5	25
$\tilde{A}\,^2T_2$		12.6_4	25
	$GeCl_3^+ + Cl$	12.3	

TABLE I. (*continued*).

Neutral/parent ion	Dissociation channel	Energy (eV)[a]	Reference
$GeCl_4^+$ $\tilde{X}\,^2T_1$		11.8_8	25
$GeCl_4$ $\tilde{X}\,^1A_1$		0	

[a] The photoelectron data (Refs. 21–25) quote adiabatic ionization potentials. The second decimal point should be treated with caution.
[b] Vertical IP (adiabatic not quoted).

Ref. 15). The electrons which provide the start pulses can therefore originate from photoionization of MX_4 to several different electronic states of the parent ion, and this is the main difficulty in extracting kinetic-energy releases from the widths of the fragment ions in the TOF spectra (Sec. V). We note that with this apparatus Stankiewicz *et al.*[18] estimate that electrons are collected with 100% efficiency so long as their kinetic energy < 7.9 eV. Similarly, ions (irrespective of their mass) are all collected if their kinetic energy < 8.8 eV.

III. ENERGETICS OF THE IONIC STATES OF MX_4 AND THEIR DISSOCIATION CHANNELS

The valence molecular orbitals of MX_4 arise from overlap of the halogen *ns, np* orbitals with the central atom valence orbitals *ms, mp*. (Thus with SiF_4, for example, overlap is between F 2*s*, 2*p* and Si 3*s*, 3*p*.) The central atom *d* orbitals play only a minor role in the bonding. The electron configuration corresponding to the five highest occupied molecular orbitals is ... $(2a_1)^2\,(2t_2)^6\,(1e)^4\,(3t_2)^6\,(1t_1)^6$. The numbering scheme does not include core orbitals. He I and He II photoelectron spectroscopy show that the five electronic states of the monopositive ion MX_4^+ all lie below 30 eV. These states have symmetry $\tilde{X}\,^2T_1$, $\tilde{A}\,^2T_2$, $\tilde{B}\,^2E$, $\tilde{C}\,^2T_2$, and $\tilde{D}\,^2A_1$, corresponding to electron removal from the $1t_1$, $3t_2$, $1e$, $2t_2$, and $2a_1$ molecular orbitals, respectively. The adiabatic ionization potentials (IPs) of these states of MX_4^+ are given for the five tetrahedral molecules studied in Table I. The data are taken from Refs. 21–25. Since the work described in this paper concerns energy thresholds, we quote adiabatic (rather than vertical) IPs. The energies of the ionic dissociation channels of MX_4 are also given in Table I. These thermodynamic energies are calculated from heats of formation of the neutrals and ionization potentials of the fragments. Full details of these calculations and the sources of the data are given in Sec. III of our two earlier publications.[4,14] Thus, for example, the energy of the $CF_2^+ + F_2$ channel is calculated from the CF_4 and CF_2 heats of formation and the ionization potential of CF_2. Since some of the thermodynamic data and IPs of the fragments are old measurements, the energies of the dissociation channels in eV are only quoted to one decimal point. The adiabatic IPs of the parent tetrahedral molecules are quoted to two decimal points although in many cases the second figure should be treated with caution. This is because of the well-known difficulty of measuring accurately an adiabatic IP when the vibrational origin band is not resolved.

In the light of our previous studies of radiative decay in MX_4^+,[4,14] several points about Table I should be noted. First, for all five group IV tetrahalides the $MX_3^+ + X$ threshold lies close to the ground electronic state of MX_4^+, and in fact MX_3^+ is always the strongest peak in the mass spectrum fragmentation pattern of MX_4. (The parent ion peak is always very weak, and with CF_4 the $m/e = 88$ peak has only recently been observed for the first time in a mass spectrometer.[26]) Second, several dissociation channels are energetically open to the $\tilde{C}$ and $\tilde{D}$ states of MX_4^+, so observation of radiative decay from these states is a surprising phenomenon. For example, CF_4^+ $\tilde{C}\,^2T_2$ lies above channels dissociating to CF_3^+ and CF_2^+, yet this state is known to fluoresce (although its quantum yield is probably less than unity).[14] Its $\tilde{D}\,^2A_1$ state at 25.1_2 eV has six different ionic channels open to it, yet it fluoresces strongly (almost certainly with unity quantum yield). Third, the fluorides and chlorides behave very differently. For example, the $\tilde{D}\,^2A_1$ state of CCl_4^+ has the same equivalent six dissociation channels open that are open to CF_4^+ $\tilde{D}\,^2A_1$, yet it decays as one might expect nonradiatively to one (or more) of these channels. Fourth, the carbon tetrahalide (fluoride or chloride) behaves differently from the equivalent silicon or germanium tetrahalide. For example, the $\tilde{C}\,^2T_2$ state of $SiCl_4^+$ and $GeCl_4^+$ both decay radiatively (probably with unity quantum yield) with a long radiative lifetime (38 and 65 ns, respectively).[14] Dissociation to $SiCl_3^+ + Cl$ is open to the former parent ion, to $GeCl_3^+ + Cl$ and $GeCl_2^+ + Cl_2$ to the latter; yet, the $\tilde{C}\,^2T_2$ state of CCl_4^+ decays nonradiatively, with six ionic channels energetically open. Similarly, the $\tilde{C}\,^2T_2$ state of SiF_4^+ decays nonradiatively (presumably to $SiF_3^+ + F$ as only this channel is open), whereas CF_4^+ $\tilde{C}\,^2T_2$ decays radiatively even though three channels are now open.

IV. NONRADIATIVE DECAY CHANNELS OF MX_4^+

A. CF_4^+

Nonradiative decay of CF_4 excited by vacuum UV radiation was studied between 480 and 820 Å (25.8 and 15.1 eV, respectively). Thus fragmentation was probed from below the energy of the $\tilde{X}$ state to above that of the $\tilde{D}$ state. The range was covered in six wavelength scans of ~ 70 Å each, with a small 10–15 Å overlap between scans. Extensive signal averaging up to the same accumulated photon count on the normalization photomultiplier tube was obtained from 480 to 640 Å (25.8–19.4 eV). This covers the region from below the energy of the $\tilde{C}$ state to above that of the $\tilde{D}$ state of CF_4^+ where fragmentation has not been studied. Less-extensive signal averaging was obtained for the region 640–820 Å (19.4–15.1 eV), since fragmentation of CF_4^+ (to $CF_3^+ + F$) in this energy range has been studied in detail by others.[5,6] The color three-dimensional map incorporating all six wavelength scans "spliced" together can be found elsewhere.[20] Two prominent ion peaks only are observed at TOFs of 4.10 and 4.82 μs. Simple calculations for our TOF spectrometer show that they correspond to ions with m/e of 50 and 69 respectively, i.e., CF_2^+ and CF_3^+. Kinetic-energy release is associated with both ion peaks, and they have half widths of 0.14 and 0.19 μs, respectively (considered in detail in Sec. V).

At a particular wavelength, the integrated signal from

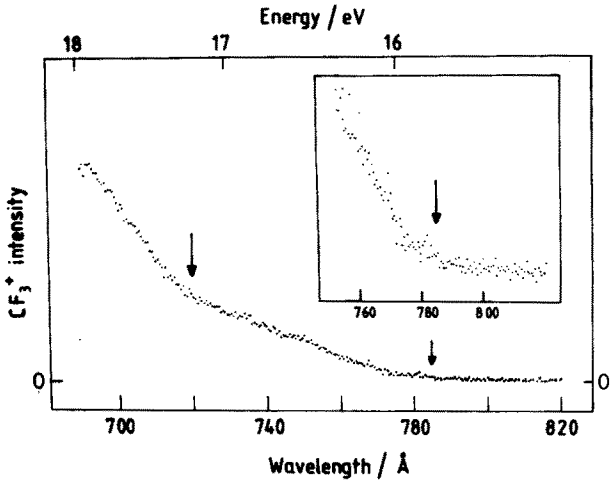

FIG. 2. A plot of the photoionization yield of CF_3^+ from CF_4 against photon wavelength in the range 690–820 Å. The two thresholds for CF_3^+ production are marked.

4.66 to 5.01 μs is a numerical representation of the CF_3^+ ion intensity. This is plotted against photon wavelength in Fig. 2 for the range 690–820 Å. Two distinct thresholds are observed at 785 ± 5 and 720 ± 5 Å (15.8 ± 0.1 and 17.2 ± 0.1 eV), and we note that the adiabatic IPs of CF_4^+ $\tilde{X}\,^2T_1$ and $\tilde{A}\,^2T_2$ are 15.3_5 and 17.1_0, respectively. The CF_3^+ intensity continues to rise for $570 < \lambda < 690$ Å, whereas for $\lambda < 570$ Å the signal remains approximately constant. There are no apparent new thresholds for CF_3^+ ion production at the adiabatic IP of the $\tilde{B}\,^2E$ (677 Å), $\tilde{C}\,^2T_2$ (571 Å), and $\tilde{D}\,^2A_1$ (493 Å) states. For $\lambda > 780$ Å there is a very small CF_3^+ signal which arises due to second-order radiation from the Seya. The effect is unimportant for lower wavelengths. The integrated signal from 4.03 to 4.16 μs represents the CF_2^+ ion intensity. In Fig. 3 this is plotted against wavelength for the range 480–640 Å. A threshold is observed at 572 ± 5 Å (21.7 ± 0.2 eV), and we note that the adiabatic IP of CF_4^+ $\tilde{C}\,^2T_2$ is 21.7_0 eV. The apparent curvature in the rise of the CF_2^+ signal above threshold may be a manifestation of the broad Franck–Condon envelope when CF_4 is photoionized to vibrational levels of CF_4^+ $\tilde{C}$.[10] For $\lambda > 640$ Å, the CF_2^+ signal remains unmeasurable above its noise level. No new threshold for CF_2^+ production can be discerned at the $\tilde{D}\,^2A_1$ state adiabatic IP of 493 Å. The ratio of the CF_2^+ to CF_3^+ ion intensities have been measured at wavelengths between 480 and 640 Å, and these data are discussed in Sec. VI A.

B. SiF_4^+

Fragmentation of SiF_4 excited by vacuum ultraviolet radiation was studied between 550 and 775 Å (22.5–16.0 eV), that is from just below the energy of the $\tilde{X}$ state to above that of the $\tilde{D}$ state of SiF_4^+. This range was covered in four equal wavelength scans of ~70 Å each, with a small overlap between scans. Extensive signal averaging was accumulated for the range 550–670 Å (22.5–18.5 eV) from below the energy of the $\tilde{C}$ state to above that of the $\tilde{D}$ state. Less extensive averaging was obtained for the lower-energy range 655–775 Å (18.9–16.0 eV). There is only one prominent ion peak at a TOF of 5.34 μs, corresponding to $m/e = 85$ or SiF_3^+, and a much weaker peak at 5.89 μs ($m/e = 104$ or SiF_4^+). SiF_2^+ is not observed over this photon range. In Fig. 4 the intensity of the SiF_3^+ ion (integrated between 5.26 and 5.45 μs) is shown as a function of photon wavelength between 655 and 775 Å. Two distinct thresholds are observed at 763 ± 5 and 718 ± 5 Å (16.2 ± 0.1 and 17.3 ± 0.1 eV). The latter figure is in excellent agreement with the adiabatic IP of SiF_4^+ $\tilde{A}\,^2T_2$ of 17.3_0 eV. The former energy is slightly greater than the $\tilde{X}\,^2T_1$ adiabatic IP, but we note that it is in excellent agreement with the thermodynamic threshold to $SiF_3^+ + F$ (Table I). For $550 < \lambda < 655$ Å the SiF_3^+ signal is approximately constant, and in particular we can discern no increase in production of this ion around the SiF_4^+ $\tilde{C}$ state IP of 642 Å (19.3 eV). This is disappointing because this state is known to have an unmeasurably low fluorescence quantum yield,[14] so nonradiative decay must dominate. Energetically $SiF_3^+ + F$ is the only accessible channel (Table I), and therefore we would expect to observe an increase in the SiF_3^+

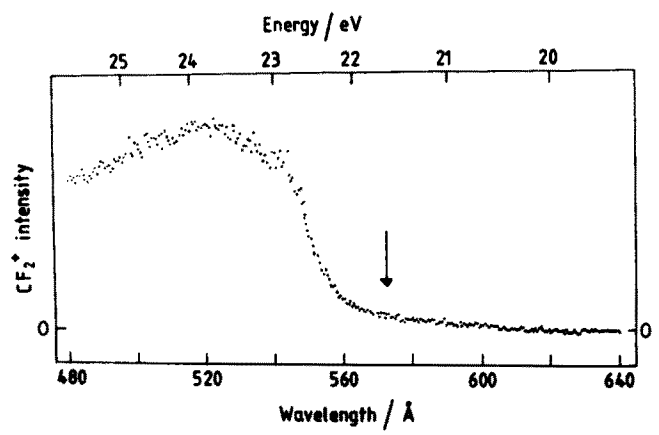

FIG. 3. A plot of the photoionization yield of CF_2^+ from CF_4 against photon wavelength in the range 480–640 Å. The threshold for CF_2^+ production is marked.

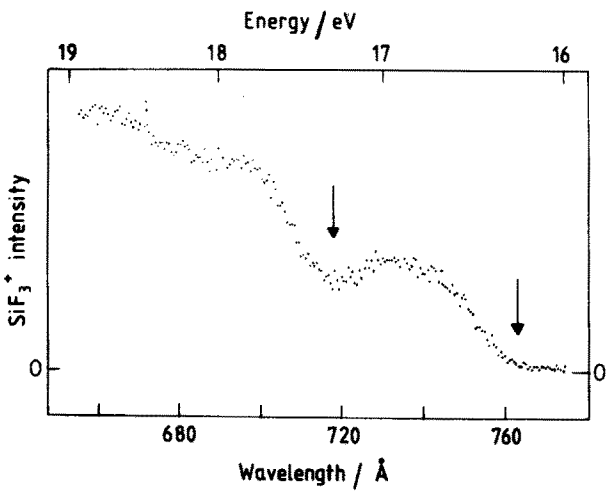

FIG. 4. A plot of the photoionization yield of SiF_3^+ from SiF_4 against photon wavelength in the range 655–775 Å. The two thresholds for SiF_3^+ production are marked.

ion signal at this energy. This highlights particularly well one limitation of our experiment. As mentioned in Sec. II, in this PEPICO apparatus there is no energy analysis of the photoelectrons. Thus at a particular photon energy where several electronic states of SiF_4^+ (in this instance) are accessible, the SiF_3^+ signal has contributions from all the different electronic states which fragment to $SiF_3^+ + F$. Since the sum of the partial ionization cross sections into SiF_4^+ $\tilde{X}$, $\tilde{A}$, and $\tilde{B}$ is much greater than into $\tilde{C}$ around 20 eV,[27] our experiment is attempting to observe a small increase in SiF_3^+ signal against a very much larger "background" signal. This point is discussed in more detail in Sec. VI. The parent ion SiF_4^+ signal (integrated between 5.81 and 5.99 μs) turns on at 770 $\pm$ 10 Å (16.1 $\pm$ 0.2 eV), in excellent agreement with the adiabatic IP of its $\tilde{X}\,^2T_1$ state.

C. CCl_4^+

Photofragmentation of CCl_4 was studied between 560 and 790 Å (22.1–15.7 eV) in four equal scans of ~70 Å each, with a small overlap between scans. Signal averaging was performed up to the same accumulated photon count in the four scans. This range covers from below the $\tilde{C}\,^2T_2$ state adiabatic IP to above that of the $\tilde{D}\,^2A_1$ state. Limited data only are collected for $\lambda > 790$ Å, because the output from the Seya monochromator was very weak. This region is where the $\tilde{X}$, $\tilde{A}$, and $\tilde{B}$ states of CCl_4^+ have their IPs. However,the energetics in Table I show that these states can only dissociate by loss of a chlorine atom to $CCl_3^+ + Cl$, and no other dissociation channels are accessible. Over the range 560–790 Å, three peaks are present in the three-dimensional map at TOFs of 4.00, 5.29, and 6.30 μs.[20] They correspond to CCl^+, CCl_2^+, and CCl_3^+, respectively. All three peaks show extensive broadened widths. This is due to both kinetic-energy release in the fragmentation and the effect of the two chlorine isotopes (^{35}Cl and ^{37}Cl in the ratio 3:1) (see Sec. V). The CCl_3^+ peak is present over the complete range, whereas the CCl_2^+ peak is only present for $\lambda < 760$ Å and CCl^+ for $\lambda < 645$ Å.

In Fig. 5 the intensity of the CCl^+ ion (integrated between 3.90 and 4.09 μs) is shown as a function of photon wavelength between 560 and 680 Å. A Threshold for ion production is observed at 645 $\pm$ 5 Å (19.2 $\pm$ 0.2 eV), and there appears to be a second enhancement in the ion signal at 625 $\pm$ 5 Å (19.8 $\pm$ 0.2 eV). The vertical IP of the $\tilde{D}\,^2A_1$ state of CCl_4^+ is 19.9 eV (or 623 Å),[24] and although an adiabatic IP is not quoted we estimate it to be 19.3 $\pm$ 0.2 eV from the spectrum of this band. Thus the CCl^+ ion appears at the adiabatic IP of the D state of CCl_4^+, and there is an enhancement in the signal at the $\tilde{D}$ state vertical IP. In Fig. 6 the intensity of the CCl_2^+ ion (integrated between 5.18 and 5.37 μs) is shown as a function of wavelength between 640 and 790 Å; for $\lambda < 640$ Å the signal remains approximately constant. A threshold at 760 $\pm$ 5 Å (16.3 $\pm$ 0.1 eV) is observed, and we note that the adiabatic IP of the $\tilde{C}$ state of CCl_4^+ is 16.3 eV or 758 Å. The CCl_3^+ signal is approximately constant between 560 and 790 Å. The relative intensities of the CCl^+ to CCl_2^+ to CCl_3^+ ion signals have been measured at wavelengths below 760 Å; these data are shown in Table II and discussed in Sec. VI C. We note that partial ionization

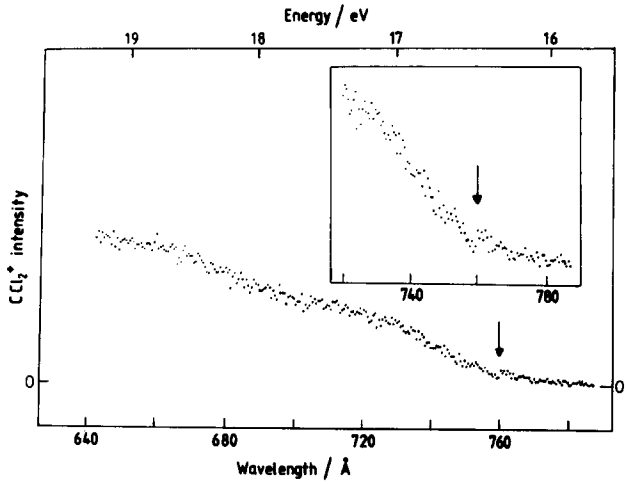

FIG. 6. A plot of the photoionization yield CCl_2^+ from CCl_4 against photon wavelength in the range 640–790 Å. The threshold for CCl_2^+ production is marked.

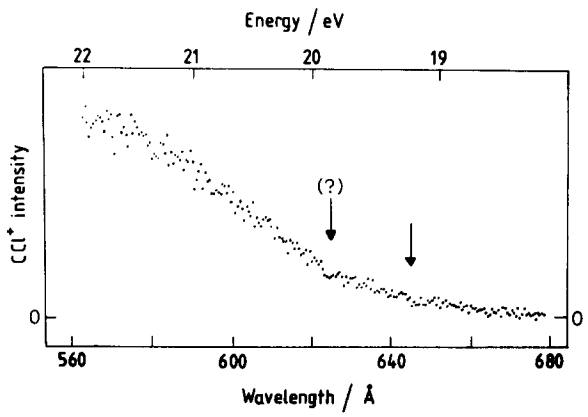

FIG. 5. A plot of the photoionization yield of CCl^+ from CCl_4 against photon wavelength in the range 560–680 Å. The threshold(s) for CCl^+ production are marked.

TABLE II. Relative photoionization yields of CCl^+, CCl_2^+, and CCl_3^+ from CCl_4 at different photon wavelengths.[a]

λ (Å)	CCl^+	CCl_2^+	CCl_3^+
560	22	32	87
584	18	35	77
600	13	36	85
620	5	39	85
640	2	33	87
660		29	85
680		24	90
700		14	87
720		13	100[b]
740		6	98

[a]The ion signals are integrated between approximately $\lambda - 2$ and $\lambda + 2$ Å.
[b]The ion intensities are ratioed to the largest CCl_3^+ signal (value = 100).

cross sections into the valence electronic states of CCl_4^+ have been measured at a limited number of photon energies in the range 560–790 Å.[28]

D. $SiCl_4^+$

Photofragmentation of $SiCl_4^+$ was studied between 650 and 840 Å (i.e., 19.1–14.7 eV) in three equal scans of ~70 Å each. Again, this covers the range from below the energy of the $\tilde{C}$ state to above that of the $\tilde{D}$ state. Extensive signal averaging was performed over the two wavelength ranges (650–720 and 770–840) Å) which encompass the energies of the $\tilde{C}$ and $\tilde{D}$ states of $SiCl_4^+$. No data was collected for $\lambda > 840$ Å because of the weak output of the Seya monochromator. This latter region is where the $\tilde{X}$, $\tilde{A}$, and $\tilde{B}$ states of $SiCl_4^+$ have their IPs. However, exactly as with CCl_4^+, these states can only dissociate by loss of a chlorine atom to $SiCl_3^+ + Cl$, and no other channels are accessible (Table I). Over the range 650–840 Å only two peaks are apparent in the three-dimensional (3D) color map at TOFs of 6.74 and 7.52 μs. They correspond to $SiCl_3^+$ and the parent ion $SiCl_4^+$, respectively. By plotting the intensity of the integrated $SiCl_3^+$ or $SiCl_4^+$ peaks against wavelength, no discernible change in either ion can be observed at the energies of the $\tilde{C}\,^2T_2$ and $\tilde{D}\,^2A_1$ states of $SiCl_4^+$. In addition, cross-section cuts at fixed photon energies were taken above and below the $\tilde{C}$ state (see Sec. II), and this also established that no new fragmentation channel was occurring from this state. The absence of a new threshold at the $\tilde{C}$ state is not surprising because this state decays radiatively, almost certainly with unity quantum yield.[4] The $\tilde{D}$ state, however, does not fluoresce, so it must dissociate nonradiatively. The branching ratio into this state at energies above its threshold is very small,[29] and no new dissociation channel is immediately apparent from the 3D color map.[20] However, by taking cuts through the histogram at fixed photon energies, a threshold to $SiCl_2^+$ is observed for energies above the $\tilde{D}$ state of $SiCl_4^+$. This threshold is measured to be 680 ± 10 Å (18.2 ± 0.2 eV). This value is slightly greater than the quoted adiabatic IP of $SiCl_4^+$ $\tilde{D}\,^2A_1$.[25] However, our value is in excellent agreement with that obtained (18.1 eV) from the convergence of a Rydberg series of $SiCl_4$ to the $\tilde{D}$ state of the parent ion,[4] and thus we believe 18.1 ± 0.2 eV to be a more reliable figure for the $\tilde{D}$ state adiabatic IP.

E. $GeCl_4$

Photofragmentation of $GeCl_4$ was studied between 650 and 850 Å. In previous experiments,[4] we established that the $\tilde{C}\,^2T_2$ and $\tilde{D}\,^2A_1$ excited electronic states of $GeCl_4^+$ and $SiCl_4^+$ showed similar radiative decay behavior: radiative decay from the $\tilde{C}$ state with a long fluorescence lifetime and unity quantum yield, but nonradiative decay from the $\tilde{D}$ state. Thus a similar fragmentation pattern to that observed in $SiCl_4^+$ was anticipated. This was indeed the case. Two ion channels are evident over the complete wavelength range studied at TOFs of 7.77 μs ($GeCl_3^+$) and 8.53 μs ($GeCl_4^+$). No discernible change in the intensity of either ion can be observed at the wavelength of the $\tilde{C}$ and $\tilde{D}$ states of $GeCl_4^+$ (851 and 680 Å, respectively). By comparing TOF spectra, above and below the $\tilde{D}$ threshold, two new channels turn on for $\lambda < 680$ Å at TOFs of 6.31 μs ($GeCl^+$) and 6.96 μs ($GeCl_2^+$). Over the limited wavelength range 650–680 Å, the relative yields of these two ions are estimated to be 1:1, although this ratio could be in error by up to 50%. The signals are weak presumably because the partial ionization cross section into the $\tilde{D}$ state is very small for these photon energies. Dissociation to these ions is thermodynamically possible (Table I). This is the only state of MX_4^+ studied where we have been able to observe a competition between two different fragmentation channels.

V. KINETIC-ENERGY RELEASE DISTRIBUTIONS OF FRAGMENT IONS

In conventional, fixed photon energy PEPICO experiments,[15] photoelectrons from an ionization event are detected after energy analysis, photoions after mass analysis. The fate of excited molecular ions can then be studied as a function of their initial, internal energy, and the fragmentation mass spectrum can be used to determine a kinetic-energy release distribution. Simplistically, a spread in ion flight times can be attributed to a range of kinetic-energy (KE) releases of the fragments—the broader the peak, the greater the KE release. Usually either an electrostatic energy analyzer or a threshold electron detector is used. In our experiments, however, no energy selectivity of the electron is incorporated into the apparatus; the photoelectron is only used as a "start" signal. This means that fragment ions evolving from different parent ionic states are all collected with a large range of initial kinetic energies, and this scrambles the available information. Because many factors contribute to an experimental width of a fragment ion, complete deconvolution to obtain a single KE release is not possible. Such factors would include thermal broadening, isotope broadening, kinematic compression, and anisotropic effects.[30]

We believe, however, that we have been able to allow for the effects of thermal broadening quite successfully. The widths of several parent ions were measured accurately in our experiment, and KE broadening will be absent for such ions. Three of the five tetrahedral molecules studied give parent ion peaks in the TOF mass spectra (SiF_4^+, $SiCl_4^+$, and $GeCl_4^+$). Three lighter ions were also measured (O_2^+ at 20.28 eV, CO_2^+ and SO_2^+ both at 23.38 eV). All the peaks are asymmetric with a tail to long time of flight. This is surprising because parent ion peaks in a Wiley–McLaren mass spectrometer should have a symmetric, Gaussian profile.[30,31] The most likely explanation is that the poor focusing of the vacuum UV radiation from the Seya monochromator into the TOF mass spectrometer means that the interaction region is quite large. Although the electric fields were optimized to fulfill the spatial focusing condition,[19] we do not believe that they can accommodate such a large interaction volume. In addition, field penetration around the ion detector may be a contributing cause of the asymmetric line shape. The half-widths (measured with a common criterion) are listed in the top half of Table III, and as expected they increase linearly with $M^{1/2}$ where M is the mass of the parent ion.[30,31] However, there are two interesting observations. First, the gradient of the half-width against $M^{1/2}$

TABLE III. Parent and fragment ion broadening in the time-of-flight mass spectra due to kinetic-energy release.

Ion	Precursor	E (eV)	M (amu)[a]	FWHM (ns)			KE of ion (eV)	Total KE release (eV)
				Observed	Thermal	KE release		
O_2^+	O_2	20.28	32	42	42	0	0	0
CO_2^+	CO_2	23.38	44	60	60	0	0	0
SO_2^+	SO_2	23.38	64	96	96	0	0	0
SiF_4^+	SiF_4	22.13	104	160	160	0	0	0
$SiCl_4^+$	$SiCl_4$	19.07	170	222	222	0	0	0
$GeCl_4^+$	$GeCl_4$	19.07	216	264	264	0	0	0
O^+	O_2	20.28	16	92	0	92	0.75	1.50
CF_2^+	CF_4	23.83	50	140	72	120	0.41	0.95[b]
CF_3^+	CF_4	23.83	69	192	103	162	0.54	2.50
SiF_3^+	SiF_4	22.13	85	146	126	74	0.09	0.49
CCl^+	CCl_4	21.93	47.5	192	70	179	0.96	[c]
CCl_2^+	CCl_4	21.93	83	212	123	173	0.51	1.11[d]
CCl_3^+	CCl_4	21.93	118.5	240	166	173	0.36	1.56
$SiCl_3^+$	$SiCl_4$	19.07	134.5	216	184	113	0.14	0.67
$GeCl_3^+$	$GeCl_4$	19.07	180.5	244	232	76	0.05	0.30

[a] Assumes Cl = 35.5 amu, Ge = 74.0 amu. The masses of the other atoms are of their principle isotope.
[b] Assumes the other fragment is F_2 (and not F + F).
[c] Total KE release cannot be determined, due to three-body fragmentation.
[d] Assumes the other fragment is Cl_2 (and not Cl + Cl).

graph is compatible with a gas translational temperature much greater than room temperature. Second, the intercept on the y axis at $M^{1/2} = 0$ occurs at negative half-width, rather than the small positive value expected.[32] Thus this graph should only be regarded as an empirical relationship from which it is possible to deconvolute the effect of thermal energy from the broadening of a fragment ion peak.

The bottom half of Table III shows the fragment ion peaks which have been studied in detail in this work. The photon energy at which the width of the peak is measured is shown in column 3, the observed half-width in column 5. The thermal contribution is shown in column 6 (using the empirical relation described above). To obtain the broadening due to KE release (column 7), we make the assumption that the peaks are Gaussian, and therefore $(\mathrm{FWHM}_{\mathrm{KE\ release}}) = [(\mathrm{FWHM}_{\mathrm{obs}})^2 - (\mathrm{FWHM}_{\mathrm{thermal}})^2]^{1/2}$ (where FWHM denotes full width at half maximum).[32] To convert this broadening (in ns) to an energy release (in eV), we note that for a Wiley–McClaren mass spectrometer $\mathrm{FWHM}_{\mathrm{KE}} \propto (\mathrm{KE})^{1/2} M^{1/2}$.[19] The $O_2 \rightarrow O^+ + O$ fragmentation via the O_2^+ $B\,^2\Sigma_g^-$ $v = 0$ state at 20.28 eV has been well studied,[33] and has a single-valued KE release of 1.50 eV (0.75 eV into the O^+ fragment). Thus it is possible to establish the constant of proportionality in the above equation as 26.56 ns $\mathrm{eV}^{-1/2}$ $\mathrm{amu}^{-1/2}$. We can therefore obtain the KE releases in the fragment ions (column 8), and by conservation of momentum the total KE release (column 9). Because the kinetic energy of the electron is not defined, for any fragment ion the KE release arises from the fragmentation of many different vibronic states of the parent ion. Thus if we consider fragmentation of CF_4 to $CF_2^+ + F_2$ (or F + F) + e^- at 23.83 eV above the CF_4^+ $\tilde{C}$ threshold of 21.70 eV, the KE release is a convolution of the contributions from different vibrational levels of CF_4^+ $\tilde{C}$. For fragmentation to $CF_3^+ + F + e^-$ at 23.83 eV, the situation is much more complicated; the KE release is a convolution of contributions from different vibrational levels of CF_4^+ $\tilde{X}$, $\tilde{A}$, and $\tilde{B}$.

The CF_3^+ result complements those of Brehm *et al.*[5] and Simm *et al.*[6] In these earlier experiments a He I discharge lamp and photoelectron energy analyzer were used to define the internal energy of the CF_4^+ parent ion, and the highest electronic state accessed was the $\tilde{B}\,^2E$ state at 18.6 eV. At this energy the total KE release in the fragmentation to $CF_3^+ + F$ does not take a single value, but is a convolution of several values between 0.4 and 2.0 eV.[6] When the $\tilde{A}\,^2T_2$ or $\tilde{X}\,^2T_1$ states are accessed smaller KE releases of ~1.3 and 1.0 eV, respectively, are measured.[5] Our value of 2.5 eV when the photon energy is 23.8 eV is compatible with these results, although as mentioned above the internal energy of CF_4^+ is not uniquely defined in our experiment. A possible way to circumvent the lack of electron energy analysis would be to measure the KE release just above and just below a threshold, and take the difference between the two TOF distributions. This has not been attempted.

The result for CF_2^+ is new. From the measured KE release in the CF_2^+ ion, it is not possible to distinguish between fragmentation to $CF_2^+ + F + F$ (energy = 20.8 eV) or $CF_2^+ + F_2$ (19.2 eV). The peak in the CF_4^+ $\tilde{C}$ state Franck–Condon envelope occurs at ~22.2 eV,[10] and therefore the most probable contribution to the CF_2^+ KE will involve a maximum total KE release of either 1.4 eV (F + F) or 3.0 eV (F_2). Some of the available energy, however, may be channeled into vibration and rotation of the molecular fragments, so from the measured translational energy release of 0.95 eV (Table III) it is not possible to distinguish the two

channels. The fact that the fragmentation is so slow (Sec. VI A) does perhaps suggest that one of the products involves the formation of a new chemical bond (i.e., $CF_2^+ + F_2$), but further experiments with some form of electron energy analyzer are needed to verify this.

Next we discuss the KE releases in CCl^+ and CCl_2^+. Fragmentation to either $CCl^+ + Cl_2 + Cl$ or $CCl^+ + Cl + Cl + Cl$ is a multibody dissociation process in which the KE release in the CCl^+ ion is not uniquely defined. The thermodynamic energies of these two channels are 16.3 and 18.8 eV, respectively, and the CCl^+ ion turns on at the $\tilde{D}\,^2A_1$ state of CCl_4^+ (vertical IP = 19.9 eV). We comment that our measured KE release of 0.96 eV in CCl^+ is more compatible with a maximum total KE release of 3.6 eV than with 1.1 eV. Therefore we suggest that CCl_4^+ $\tilde{D}$ fragments to $CCl^+ + Cl_2 + Cl$. The discussion used above for fragmentation of CF_4^+ $\tilde{C}$ can be applied to fragmentation of CCl_4^+ $\tilde{C}$ to either $CCl_2^+ + Cl_2$ or $CCl_2^+ + Cl + Cl$. The total KE release of 1.1 eV suggests that $CCl_2^+ + Cl_2$ is the more likely product, although we cannot rule out the latter channel. A conventional PEPICO experiment with He I radiation[15] could resolve this problem.

The KE releases for the fragmentations to SiF_3^+, CCl_3^+, $SiCl_3^+$, and $GeCl_3^+$ are all new values. In each of these cases the thermodynamic limit for the $MX_3^+ + X$ channel lies up to 1 eV above the ground-state adiabatic IP of the parent ion MX_4^+ (Table I). Therefore substantially smaller KE releases are expected from the $\tilde{X}$, $\tilde{A}$, and $\tilde{B}$ states of these ions compared to the fragmentation of the equivalent states of CF_4^+ (see above), where the $CF_3^+ + F$ channel lies 0.65 eV below the adiabatic IP of CF_4^+ $\tilde{X}$. With the exception of CCl_4^+, this appears to be the case (Table III), and we note that SiF_4^+, $SiCl_4^+$, and $GeCl_4^+$ all show a parent ion peak in their TOF spectra. CCl_4^+ does not show such a peak, and the measured KE release for fragmentation to $CCl_3^+ + Cl$ is as large as 1.56 eV. If the energetics in Table I are correct, this is higher than expected since 11.8 eV (the energy of $CCl_3^+ + Cl$) + 1.56 eV (the measured KE release) = 13.36 eV, which is close to the adiabatic IP of CCl_4^+ $\tilde{B}$. Yet the measured KE release will include contributions from the lower-energy $\tilde{X}$ and $\tilde{A}$ states, and they will be weighted heavily by their large partial ionization cross sections.[28] Therefore either the measured KE release is in error, or the thermodynamic energy for CCl_3^+ production is too high. The latter explanation is possible, since this energy is an appearance potential for CCl_3^+ from CCl_4,[34] and therefore is an upper bound. Clearly all these KE releases could be usefully remeasured in a conventional PEPICO experiment using He I radiation, with the advantages described above.

VI. DISCUSSION

A. CF_4

Our results show that the $\tilde{X}$, $\tilde{A}$, and $\tilde{B}$ electronic states of CF_4^+ all dissociate by loss of a fluorine atom to $CF_3^+ + F$, and we note from Table I that this is the only ionic dissociation channel energetically available. The CF_3^+ ion signal turns on at 15.8 eV, which lies above the adiabatic energy of the $\tilde{X}\,^2T_1$ state of CF_4^+, rather than at its thermodynamic energy (14.7 eV). Thus dissociation of CF_4^+ $\tilde{X}$ is direct and rapid, and this explains the continuous nature of the CF_4^+ $\tilde{C}$–$\tilde{X}$ fluorescence spectrum.[7] Dissociation of the $\tilde{A}$ state is likewise direct, so fluorescence bands of CF_4^+ terminating in the $\tilde{A}$ state are also broad and continuous.[7] These observations are compatible with the fact that both $\tilde{X}$ and $\tilde{A}$ states show no structure in their photoelectron spectra. Partial vibrational structure is observed in the $\tilde{B}\,^2E$ photoelectron band,[21] but it has been shown that radiative decay from this state is a very minor pathway.[35] Thus a nonradiative process dominates, and our work shows that this is fragmentation to $CF_3^+ + F$. It is not possible to say whether this state dissociates directly or by some slightly slower predissociation mechanism. Our results complement those of Brehm *et al.*[5] and Simm *et al.*[6] We have measured fragmentation of CF_4^+ continuously as a function of excitation energy from below the energy of the $\tilde{X}$ state to above that of the $\tilde{D}$ state, whereas measurements of these other two groups were made only at a few specific energies below the He I energy of 21.22 eV. However, by energy analysis of the photoelectron, they could measure the KE release in the CF_3^+ fragment much more accurately.

The results reported here for energies > 20 eV are new. The CF_4^+ $\tilde{C}\,^2T_2$ state shows well-resolved vibrational structure in its photoelectron band,[22] and decays radiatively via bound–free $\tilde{C}$–$\tilde{A}$ and $\tilde{C}$–$\tilde{X}$ emission.[7] In our earlier fluorescence work,[14] we estimate that the fluorescence quantum yield of this state is only ~0.5. Thus a nonradiative channel is competing with radiative decay. The decrease in the radiative lifetime of the $\tilde{C}$ state with excitation energy[14] also shows the presence of a competing nonradiative channel. Our results show that this channel is fragmentation to CF_2^+, and this process must be slow (on the ns time scale) because fluorescence (τ_{rad} = 9 ns) can compete. Unfortunately, it is not possible to say whether the other product is F_2 or F + F. The former would involve a total KE release of 2.5 eV, the latter 0.9 eV, if the lowest vibrational level of CF_4^+ $\tilde{C}$ was excited at 21.7_0 eV. However, because we do not define the internal energy of the CF_4^+ parent ion in these experiments, our measurement (0.95 eV at an excitation energy of 23.83 eV) can only give an indication of the total-energy release. Again we note that the CF_2^+ signal turns on at the CF_4^+ $\tilde{C}$ state energy (21.7 eV) and not at its lowest thermodynamic energy (19.2 eV). Our value for the CF_2^+ threshold has recently been confirmed by the lower resolution technique of dipole (e, e + ion) spectroscopy[36] (21 ± 1 eV), and both results confirm much older appearance potential data using electrons as an excitation source.[37]

An independent estimate of the fluorescence quantum yield $\Phi_{h\nu}$ of CF_4^+ $\tilde{C}$ can be made from the areas of the CF_2^+ and CF_3^+ peaks in the TOF spectra. We assume that nonradiative decay of $\tilde{C}$ only produces the CF_2^+ ion fragment, radiative decay ultimately produces CF_3^+ by direct dissociation of the $\tilde{A}$ and $\tilde{X}$ states following $\tilde{C}$–$\tilde{A}$, $\tilde{X}$ fluorescence, and these two ions are detected with equal efficiency. At any

photon energy, the area of the CF_2^+ peak to the CF_3^+ peak is then given by $\sigma_c(1-\Phi_{h\nu})/(\sigma_x+\sigma_A+\sigma_B+\sigma_C\Phi_{h\nu})$, where σ_i is the partial ionization cross section into electronic state i. These latter quantities have been measured by Carlson *et al.*[38] at several energies above the $\tilde{C}$ state threshold. Only data for $\lambda > 480$ Å ($E < 25.8$ eV) is relevant to this work. Thus by measuring the ratio of the CF_2^+:CF_3^+ integrated peak area at 23, 24, 25, and 25.8 eV, we estimate $\Phi_{h\nu} = 0.61$, 0.53, 0.54, and 0.50, respectively. Not only are the absolute values in excellent agreement with those estimated from the earlier fluorescence excitation work,[14] but the decrease in $\Phi_{h\nu}$ with increasing photon energy above the $\tilde{C}$ state threshold is also confirmed. (We note that Zhang *et al.*[36] incorrectly assign the competing decay pathway of CF_4^+ $\tilde{C}$ to direct dissociation to $CF_3^+ + F$, rather than to radiative decay of the parent ion.)

The $\tilde{D}\,^2A_1$ state of CF_4^+ has a narrow photoelectron band (with its maximum at the adiabatic IP), and decays radiatively via bound–bound ($\tilde{D}$–$\tilde{C}$) and bound–free ($\tilde{D}$–$\tilde{A}$, $\tilde{X}$) electronic transitions. The threshold for fluorescence is 25.0 eV,[14] and turns on sharply because Franck–Condon factors favor ionization to the lowest vibrational level of D. In this earlier work we used a CsI solar blind photomultiplier tube to detect $\tilde{D}$–$\tilde{A}$, $\tilde{X}$ fluorescence. Because this tube is insensitive at 391 nm, it was not possible to calibrate it with N_2^+ B–X fluorescence, and thus no estimate could be made of the $\tilde{D}$ state fluorescence quantum yield. Similarly, the count rate was so low that it was not possible to measure the radiative lifetime. Using a (nonresonant) pulsed electron beam excitation source, Hesser and Dressler measured the lifetime of CF_4^+ $\tilde{D}$ to be 2.1 ± 0.2 ns,[39] but no measurement of its variation with excitation energy was possible. By analogy with SiF_4^+ $\tilde{D}$ (see Sec. VI B) we believe the quantum yield of this state is unity, and no nonradiative processes are operative. This is consistent with the fact that no change in CF_2^+ or CF_3^+ signal is observed at the $\tilde{D}$ state adiabatic IP of 493 Å (25.1 eV). However, it should be noted that any change in fragment ion signal will be small, because the $\tilde{D}$ state partial ionization cross section at energies > 25.1 eV is much smaller than either the sum of any one of the $\tilde{X}$, $\tilde{A}$, $\tilde{B}$, and $\tilde{C}$ partial cross sections.[38] [Again, we note that Zhang *et al.*[36] incorrectly assign the only decay route of the $\tilde{D}$ state to a nonradiative process to CF^+. Although this is energetically possible (Table I), we see no evidence for the appearance of CF^+ in the TOF spectra at the adiabatic IP of the CF_4^+ $\tilde{D}$ state, and in fact, the appearance potential of CF^+ occurs at a higher energy of 30 ± 1 eV.[36]

B. SiF_4

In Sec. IV B we noted that the parent ion signal from SiF_4 turns on at the adiabatic IP of SiF_4^+ $\tilde{X}$. Fragmentation to $SiF_3^+ + F$ occurs at slightly higher energy, in excellent agreement with the thermodynamic predictions of Table I. Thus it appears that the ground state of SiF_4^+ has a shallow minimum in its potential-energy surface, which is the source of the weak but easily detectable parent ion signal in the TOF spectra. This is in contrast to CF_4^+ where the $CF_3^+ + F$ dissociation limit lies ~ 0.6 eV below the energy of CF_4^+ $\tilde{X}$ (Table I) and where the parent ion is virtually undetectable.[26] However, SiF_4^+ $\tilde{X}$ is certainly dissociative above the $SiF_3^+ + F$ threshold, as indicated by the lack of vibrational structure in the photoelectron band[23] and the continuous nature of the SiF_4^+ $\tilde{D}$–$\tilde{X}$ fluorescence spectrum.[8] The $\tilde{A}$ state of SiF_4^+ behaves similarly to that of CF_4^+. It is an unbound state [as shown by the lack of structure in the $\tilde{D}$–$\tilde{A}$ fluorescence band at 304 nm (Ref. 8)], dissociating directly and rapidly by loss of a fluorine atom to SiF_3^+. The $\tilde{B}$ state of SiF_4^+ also decays nonradiatively by loss of one fluorine atom, although this state does show partial vibrational structure in its photoelectron spectrum.[23]

The $\tilde{C}\,^2T_2$ state of SiF_4^+ shows well-resolved vibrational structure in its photoelectron band,[23] and distorts from tetrahedral geometry by a dynamic Jahn–Teller effect.[2] The $\tilde{D}$–$\tilde{C}$ emission spectrum has been studied in some detail at a low temperature in our molecular-beam apparatus,[2,10,11] and to all intents and purpose the lower $\tilde{C}$ state exhibits the properties of a bound state. Furthermore, recently we have photographed the three strongest vibronic bands of SiF_4^+ $\tilde{D}$–$\tilde{C}$ at Doppler-limited resolution.[40] Rather surprisingly, this state does not decay radiatively[14] and it was postulated that this was connected with the distorted structure of this state. Energetically, the only ionic dissociation channel accessible is $SiF_3^+ + F$ (Table I), Our experiments only confirm this indirectly, in that no new ion (e.g., SiF_2^+) turns on at the $\tilde{C}$ state adiabatic IP. It is disappointing that it is not possible to observe an increase in the SiF_3^+ signal directly, and probable reasons for this have been described in Sec. IV B. The ability to record rotational structure in the SiF_4^+ $\tilde{D}$–$\tilde{C}$ spectra at a resolution of 0.05 cm^{-1} (Ref. 40) places an upper limit on the dissociation rate of the $\tilde{C}$ state of $\sim 10^{10}$ s^{-1}. Thus the nonradiative decay of this state is relatively slow.

The $\tilde{D}$ state of SiF_4^+ behaves similarly to that of CF_4^+. Radiative decay dominates, and this is the upper state of the bound–bound ($\tilde{D}$–$\tilde{C}$) and bound–free ($\tilde{D}$–$\tilde{A}$, $\tilde{X}$) transitions in SiF_4^+. The energy threshold for fluorescence is 21.5 eV,[14] in excellent agreement with the adiabatic IP of this state.[22] In our earlier synchrotron work, we also estimated the fluorescence quantum yield of this state to lie between 0.5 and 1.0, and to be independent of energy. More significantly, the radiative lifetime of this state (9.3 ns) is also invariant to energy. This strongly suggests that no competing nonradiative channel operates and $\Phi_{h\nu}$ is unity. Thus no change in any fragment ion signal is observed at the $\tilde{D}$ state adiabatic IP in the TOF spectrum. Energetically, dissociation to $SiF_2^+ + F_2$ is now accessible (as well as to $SiF_3^+ + F$), but the SiF_2^+ ion is not observed at all in our TOF spectra.

C. CCl_4^+

The earlier fluorescence work[4] established that neither the $\tilde{C}$ nor $\tilde{D}$ states of CCl_4^+ decay radiatively. Thus rapid nonradiative processes must dominate the decay dynamics of these states. Figure 6 shows that the $\tilde{C}\,^2T_2$ state decays to CCl_2^+, since the threshold for CCl_2^+ ion production occurs at the adiabatic IP of the $\tilde{C}$ state of the parent ion. As with CF_4^+ $\tilde{C}$, it is not possible to determine the nature of the other product. Both Cl_2 and Cl + Cl are energetically possible, the

former involving a KE release of 3.0 eV, the latter 0.5 eV. It is assumed that the decay rate for this process is so rapid that it dominates any weak radiative decay. Thus if radiative decay is occurring, the fluorescence quantum yield of this state is so small that no signal can be observed in the fluorescence excitation experiment.[4] This is in contrast to the decay dynamics of CF_4^+ $\tilde{C}$ where the nonradiative decay channel (to CF_2^+) is slow enough that radiative decay can compete.

Figure 5 shows that the $\tilde{D}\,^2A_1$ state of CCl_4^+ decays nonradiatively to CCl^+, and an improved value for the adiabatic IP of CCl_4^+ $\tilde{D}$ is determined (19.2 ± 0.2 eV). The other products are probably $Cl_2 + Cl$, and energetically this process has a KE release of 2.9 eV. This behavior is in contrast to the $\tilde{D}\,^2A_1$ state of CF_4^+ and SiF_4^+ which decay radiatively, probably with unity fluorescence quantum yield. The difference between the chlorides and fluorides could be a consequence of spin-orbit coupling effects in the heavier species creating nonradiative decay channels via doublet–quartet coupling. *Ab initio* calculations have recently been reported on the positions of the five valence doublet electronic states of CF_4^+ and SiF_4^+,[41] but there have been no calculations yet on the quartet states of these ions *or* on the positions of any of the states in CCl_4^+.

We believe that the decay routes of the $\tilde{C}$ and $\tilde{D}$ states of CCl_4^+ are unique — that is, the $\tilde{C}$ state dissociates only to CCl_2^+ and the $\tilde{D}$ state only to CCl^+. No increase in the CCl_3^+ signal can be observed at the adiabatic energy of either the $\tilde{C}$ or $\tilde{D}$ state of CCl_4^+, and similarly no increase in the CCl_2^+ signal can be observed at the $\tilde{D}$ state energy. Assuming the CCl^+, CCl_2^+, and CCl_3^+ ions are all detected with equal efficiency, then at any photon energy above the CCl_4^+ $\tilde{D}$ state the ratio of the CCl^+ to CCl_2^+ to CCl_3^+ intensities should equal the ratio of σ_D to σ_C to $(\sigma_X + \sigma_A + \sigma_B)$, where σ_i is the partial ionization cross section into electronic state i. Within the wavelength range 560–790 Å, cross-section data are only available at 620 and 584 Å.[28] At 620 Å (or 20.0 eV) Carlson *et al.* predict the ratio of CCl_2^+ to CCl_3^+ to be 0.38 to 1.00, whereas we obtain 0.46 to 1.00 (Table II). At 584 Å, they obtain this same ratio to be 0.26 to 1.00, whereas we obtain 0.45 to 1.00. However, within the large error limits quoted for σ_i, the agreement between the two sets of data is enhanced. Data for σ_D are not given, so it is not possible to compare our photoionization yields of CCl^+ with those that would be predicted from the partial ionization cross sections.

D. $SiCl_4^+$

The $\tilde{C}$ state of $SiCl_4^+$ decays radiatively with a long radiative lifetime (38.4 ns) which is invariant to excitation energy.[14] This suggests strongly that the fluorescence quantum yield of this state is unity, and that no nonradiative process competes with fluorescence. Thus the absence of any change in the $SiCl_3^+$ ion intensity when the photon energy is scanned through the $SiCl_4^+$ $\tilde{C}$ adiabatic energy is not surprising. Energetically, this is the only fragment ion which can be formed from this state. The $\tilde{D}$ state decays nonradiatively, and our results show that dissociation to $SiCl_2^+$ ($+ Cl_2$ or $Cl + Cl$) is the dominant channel. (For reasons mentioned above, it is very difficult to ascertain whether there is a contribution to the $\tilde{D}$ state decay from $SiCl_3^+ + Cl$.) The parent ion is observed in the TOF spectra because the ground state of $SiCl_4^+$ lies approximately 0.9 eV below the lowest ionic dissociation channel (Table I). The minimum in the $\tilde{X}$ state potential surface must occur at a very different geometry from the $\tilde{C}$ state of $SiCl_4^+$, however, because the $\tilde{C}$–$\tilde{X}$ fluorescence band is continuous with no discrete structure.[4] This probably means that the Franck–Condon region of the $\tilde{X}$ state accessed by emission from the $\tilde{C}$ state is the repulsive part of the surface lying above the $SiCl_3^+ + Cl$ dissociation energy.

E. $GeCl_4^+$

The $\tilde{C}$ state of $GeCl_4^+$ behaves very similarly to that of $SiCl_4^+$ with long radiative lifetime (65.4 ns) which is invariant to excitation energy.[14] Thus the fluorescence quantum yield of this state is probably unity, no nonradiative processes are competing, and there is therefore no change in the $GeCl_3^+$ ion intensity when the photon energy is scanned through the $GeCl_4^+$ adiabatic potential. Energetically, dissociation to both $GeCl_3^+$ and $GeCl_2^+$ is possible from this state (Table I). The $\tilde{D}$ state of $GeCl_4^+$ decays nonradiatively, but unlike $SiCl_4^+$ there now appear to be two competing channels to $GeCl_2^+$ and to $GeCl^+$. The arguments for the presence of the parent ion $GeCl_4^+$ in the TOF spectra, and the continuous nature of the $GeCl_4^+$ $\tilde{C}$–$\tilde{X}$ fluorescence band are the same as described above for $SiCl_4^+$.

VII. CONCLUDING REMARKS

As mentioned in Sec. I, the technique described in this paper to observe non-radiative decay channels of polyatomic molecular ions has many similarities to photoionization mass spectrometry (PIMS).[16] We believe that the increased range of wavelengths available from a synchrotron source and the use of TOF detection give two considerable advantages over conventional PIMS experiments. Both techniques use photons as the excitation source, and we comment that, in general, appearance energies of fragment ions will be much more accurately determined than with techniques using electrons as the excitation source. There are two reasons for this. First, it is difficult to produce a monochromatic electron beam with well-characterized energy below 20 eV, and extrapolations from higher energy are often necessary. Second, and specifically with regard to a single ionization process to form an electronic state of the parent ion, with photon excitation the cross section usually shows a step function at the threshold energy, whereas with electrons the cross-section increases only slowly and linearly with the excess energy above threshold;[42] establishing the threshold in the latter case can therefore be difficult.

In the five tetrahedral ions studied, we observe appearance potentials of the fragment ions which are greater than the thermodynamic appearance energy of that ion. The observed appearance energy can usually be related to the adiabatic ionization potential of an electronic state of the parent tetrahedral ion. Thus the threshold for CF_2^+ production from CF_4 turns on at the CF_4^+ $\tilde{C}$ state adiabatic IP (21.7 eV)

and not at the lowest thermodynamic energy channel involving CF_2^+ (19.2 eV). This is in contrast to photoionization studies of CH_4, where the appearance energies of CH_3^+, CH_2^+, and CH^+ are at their thermodynamic values and are not related to the energetics of the electronic states of CH_4^+.[43] For such large five-atom polyatomics, the behavior of CH_4 is the more usual, and arises, we believe, because the ground electronic state of CH_4^+ $\tilde{X}\,^2T_2$ is stable with a deep minimum in its potential surface. (In fact, the surface has a double minimum due to static Jahn–Teller distortion of the state.[44]) Thus resonant autoionization via high vibrational levels of this state can play an important role. The behavior of the MX_4^+ ions described in this paper is unusual, and probably arises because of the absence of a particularly stable ground electronic state of MX_4^+. It is clear that a much fuller understanding of the dynamics of these nonradiative processes will only be obtained if detailed positions of the potential curves of both doublet and quartet valence electronic states of MX_4^+ are known. Such *ab initio* calculations are badly needed. From an experimental point of view, the main improvement to the apparatus would be to detect threshold energy electrons in coincidence with the fragment ions. It will then be possible to measure the KE release in the individual fragment channels much more accurately since the vibronic state of the parent ion will be uniquely determined.

ACKNOWLEDGMENTS

We thank Dr. O. Dutuit for communicating her results on CH_4^+ prior to publication, and for interesting discussions. The financial support of the Science and Engineering Research Council (SERC) (United Kingdom) and the Daresbury Laboratory is acknowledged. M. S. thanks SERC for a Visiting Research Fellowship; J. C. C., I. R. L., and P. A. H. thank SERC for Research Studentships.

[1] J. F. M. Aarts, S. M. Mason, and R. P. Tuckett, Mol. Phys. **60**, 761 (1987).
[2] S. M. Mason and R. P. Tuckett, Mol. Phys. **60**, 771 (1987).
[3] S. M. Mason and R. P. Tuckett, Mol. Phys. **62**, 979 (1987).
[4] I. R. Lambert, S. M. Mason, R. P. Tuckett, and A. Hopkirk, J. Chem. Phys. **89**, 2675 (1988).
[5] B. Brehm, R. Frey, A. Kustler, and J. H. D. Eland, Int. J. Mass Spectrom. Ion Phys. **13**, 251 (1974).
[6] I. G. Simm, C. J. Danby, J. H. D. Eland, and P. I. Mansell, J. Chem. Soc. Faraday Trans. 2 **72**, 426 (1976).
[7] J. F. M. Aarts, Chem. Phys. Lett. **114**, 114 (1985).
[8] J. F. M. Aarts, Chem. Phys. **101**, 105 (1986).
[9] H. van Lonkhuyzen and J. F. M. Aarts, Chem. Phys. Lett. **140**, 434 (1987).
[10] S. M. Mason and R. P. Tuckett, Mol. Phys. **62**, 175 (1987).
[11] S. M. Mason, Ph.D. thesis, University of Cambridge, 1988.
[12] K. A. Blanks and K. Becker, J. Phys. B **20**, 6157 (1987).
[13] J. Sasaki, I. Kuen, and F. Howorka, J. Chem. Phys. **86**, 1938 (1987).
[14] I. R. Lambert, S. M. Mason, R. P. Tuckett, and A. Hopkirk, J. Chem. Phys. **89**, 2683 (1988).
[15] J. H. D. Eland, J. Chem. Phys. **70**, 2926 (1979).
[16] J. Berkowitz, *Photoabsorption, Photoionisation and Photoelectron Spectroscopy* (Academic, New York, 1979); Radiat. Phys. Chem. **32**, 23 (1988).
[17] L. J. Frasinski, M. Stankiewicz, K. J. Randall, P. A. Hatherly, and K. Codling, J. Phys. B **19**, L819 (1986).
[18] M. Stankiewicz, P. Hatherly, L. J. Frasinki, K. Codling, and D. M. P. Holland, J. Phys. B **22**, 21 (1989).
[19] W. C. Wiley and I. H. McLaren, Rev. Sci. Instrum. **26**, 1150 (1955).
[20] I. R. Lambert, Ph.D. thesis, University of Birmingham (in preparation).
[21] C. R. Brundle, M. B. Robin, and H. Basch, J. Chem. Phys. **53**, 2196 (1970).
[22] D. R. Lloyd and P. J. Roberts, J. Electron Spectrosc. **7**, 325 (1975).
[23] R. Jadrny, L. Karlsson, L. Mattsson, and K. Siegbahn, Chem. Phys. Lett. **49**, 203 (1977).
[24] W. von Niessen, L. Asbrink, and G. Bieri, J. Electron Spectrosc. **26**, 173 (1982).
[25] P. J. Bassett and D. R. Lloyd, J. Chem. Soc. A 641 (1971).
[26] Y. J. Kime, D. C. Driscoll, and P. A. Dowben, J. Chem. Soc. Faraday Trans. 2 **83**, 403 (1987).
[27] B. W. Yates, K. H. Tan, G. M. Bancroft, L. L. Coatsworth, and J. S. Tse, J. Chem. Phys. **83**, 4906 (1985).
[28] T. A. Carlson, M. O. Krause, F. A. Grimm, P. Keller, and J. W. Taylor, J. Chem. Phys. **77**, 5340 (1982).
[29] T. A. Carlson, A. Fahlman, M. O. Krause, T. A. Whitley, F. A. Grimm, M. N. Piancastelli, and J. W. Taylor, J. Chem. Phys. **84**, 641 (1986).
[30] J. L. Franklin, P. M. Hierl, and D. A. Whan, J. Chem. Phys. **47**, 3148 (1967).
[31] J. H. D. Eland, Int. J. Mass Spectrom. Ion Phys. **8**, 143 (1972).
[32] I. Powis, P. I. Mansell, and C. J. Danby, Int. J. Mass Spectrom. Ion Phys. **32**, 15 (1979).
[33] M. Richard-Viard, O. Dutuit, M. Lavolee, T. Govers, P. M. Guyon, and J. Durup, J. Chem. Phys. **82**, 4054 (1985).
[34] J. B. Farmer, H. S. Henderson, F. P. Lossing, and D. G. H. Marsden, J. Chem. Phys. **24**, 348 (1956).
[35] J. P. Maier and F. Thommen, Chem. Phys. Lett. **78**, 54 (1981).
[36] W. Zhang, G. Cooper, T. Ibuki, and C. E. Brion, Chem. Phys. **137**, 391 (1989).
[37] C. Lifshitz and F. A. Long, J. Phys. Chem. **69**, 3731 (1965).
[38] T. A. Carlson, A. Fahlman, W. A. Svensson, M. O. Krause, T. A. Whitley, F. A. Grimm, M. N. Piancastelli, and J. W. Taylor, J. Chem. Phys. **81**, 3828 (1984).
[39] J. E. Hesser and K. Dressler, J. Chem. Phys. **47**, 3443 (1967).
[40] J. L. Chotin, I. R. Lambert, S. Leach, and R. P. Tuckett (unpublished).
[41] R. A. Bearda, H. R. R. Wiersinga, J. F. M. Aarts, and J. C. C. Mulder, Chem. Phys. **137**, 157 (1989).
[42] G. H. Wannier, Phys. Rev. **90**, 817 (1953).
[43] O. Dutuit, M. Alt-Kaci, J. Lemaire, and M. Richard-Viard, Phys. Scr. **T31**, 223 (1990).
[44] J. Rabalais, T. Bergman, L. O. Werme, L. Karlsson, and K. Siegbahn, Phys. Scr. **3**, 13 (1971).